

Comparative study of malachite green adsorption onto activated carbon prepared from *Ziziphus* wood and ZnO nanoparticles loaded AC: artificial neural network modeling and optimization

Aygin Mohammadi^a, Mehrorang Ghaedi^{b,*}, Mohammad Mehdi Sabzehmeidani^c

^aChemistry Department, Firuzabad Branch, Islamic Azad University, Firuzabad, Iran, email: m.aygin@yahoo.com

^bChemistry Department, Yasouj University, Yasouj 75918-74831, Iran, Tel. and Fax: +98-74-33223048; email: m_ghaedi@yu.ac.ir

^cChemical Engineering Department, Yasouj University, Yasouj, Iran, email: m.sabzehmeidani@gmail.com

Received 5 October 2017; Accepted 12 June 2018

ABSTRACT

In this study activated carbon prepared from *Ziziphus* wood was modified by ZnO nanoparticles loaded on activated carbon (ZnO-NPs-AC) and checking its applicability for malachite green (MG) removal. The properties of ZnO-NPs-AC were identified by X-ray diffraction, transmission electron microscopy, field emission scanning electron microscopy, and Brunauer–Emmett–Teller. Response surface methodology and artificial neural network (ANN) model learned with Levenberg–Marquardt algorithm are used for modeling of MG adsorption onto present support. The mean squared error and coefficient of determination (R^2) for the optimal ANN model with eight neurons at hidden layer were 0.9999 and 0.00116 by AC and 0.9970 and 0.01789 by ZnO-NPs-AC for testing data, respectively. The optimum conditions were set as 0.02 and 0.015 g for ZnO-NPs-AC and AC are applicable for successful removal of MG (97.38% and 71.35%) in reasonable time (5 min for ZnO-NP-AC and 4.65 min for AC). The adsorption isotherm is efficiently explained by Temkin and Langmuir for AC and ZnO-NPs-AC adsorbent. The adsorption kinetics of MG excellently follows the pseudo-second-order kinetic model.

Keywords: *Ziziphus* wood; ZnO-NPs-AC; Response surface methodology; Ultrasonic assisted adsorption; Artificial neural network

1. Introduction

Textile wastewaters are composed of various organic combinations such as dyes and hazardous material which are harmful to aquatic organisms. In the most cases, the presence of dyes and subsequent environmental problems are reason for generation of hazards for living organisms [1–3]. Most pigments and dyes due to their complex structure are difficult to degrade when discharged into effluent streams and lately lead to serious diseases and health problems. Malachite green (MG) has abundant industrial applications (dyeing, textile, leather, plastics, and paper industries) [4] and accordingly causes hepatotoxicity, genotoxicity, mutagenic and

carcinogenic effects on human and animals which may be responsible for some injury [5–7]. Hence, treatment of dyes containing industrial effluent attains growing interest.

Conventional wastewater treatment methods have their own advantages and limitation [8–10]. Among these methods, the adsorption process using activated carbons (ACs) that are prepared from natural agriculture source are highly recommended in terms of lower initial cost, flexibility of design, and more availability [11–14]. The physicochemical characteristics of ACs are directly related to the selected raw materials and conditions for their preparations. In the last decades, AC was supplied from various agricultural wastes such as palm-tree cobs [15], rice husks [16], olive stones [17], bagasse [18], and other sources [19–22]. The ACs can attain more features owing to their modification and/or functionalization which improve surfaces and adsorbent/adsorbate

* Corresponding author.

interactions and internal adsorption sites [23]. More efforts were devoted to preparation of carbon-based materials by nanoscale chemical substances, which are proportional with extensive modification and improvement in their performance. This modification leads to increase in accessible surface area and rate of mass transfer [24,25]. One of the most recommended pathways for AC modification is their loading by different nanostructures. The ZnO nanoparticles have great ability as ACs modifier surface to supply ZnO-NP-AC with greater active surface sites with respect to AC as alone adsorbent. On the other hand, back probable distribution of Zn^{2+} ions to environments has lower hazards for most living organisms.

Artificial neural network (ANN) is computational or mathematical model based on biological neural networks for classification, pattern recognition, modeling, and prediction of systems by data passing through the connections from one neuron to another [26,27]. The ANN approach is vastly used in various activities such as wastewater treatment to introduce mathematical functions for both nonlinear and linear systems [28,29] including adsorption [30,31], chromatography based on separation [32], and degradation [33] approaches.

In this study, the MG removal from water has been investigated using AC supplied from *Ziziphus* wood and subsequently was loaded with zinc oxide (ZnO) nanoparticles (ZnO-NPs-AC). The physical and chemical characteristics of the proposed materials were determined using field emission scanning electron microscopy (FE-SEM), transmission electron microscopy (TEM), Brunauer–Emmett–Teller (BET), and X-ray diffraction (XRD). Central composite design (CCD) applied for optimization of operational conditions such as sonication time, amount of adsorbent, and initial dye concentration and process was modeled by ANN model. Kinetics and equilibrium of adsorption were well explained by second-order kinetic model and Langmuir model.

2. Experimental

2.1. Materials and apparatus

All reagents and chemicals were obtained from Merck (Germany) and the deionized water was used for all these experiments. Table 1 illustrates the chemical structure of MG (molecular formula: $C_{23}H_{25}ClN_2$, color index number = 42,000, Mw = 364.911 g mol⁻¹ and λ_{max} = 618 nm). The *Ziziphus* woods obtained from Yasuj in Iran were crushed into smaller pieces

(measuring between 1 cm and 4 cm in length) and separately washed with doubly distilled water to remove dirt and dust particles and dried in sun. Five hundred grams of the selected fraction was heated in a hot air oven at 400°C for 2 h. The coal produced has been washed with distilled water and was heated in an oven at 100°C for 24 h until near dry. The material was crushed in a mortar and sieved to desirable particle sizes. Then it was impregnated with concentrated HNO_3 . 10 g of these carbon powder materials were suspended in 150 mL of 5M HNO_3 and refluxed at 100°C for 8 h and carbon was filtered and washed with distilled water for several times until the pH subsequently 6 and in later stage was dried at 100°C for 24 h in oven. The ZnO nanoparticles loaded was prepared according to literature and subsequently was loaded onto ACs [34]. The characterization of AC *Ziziphus* wood and ZnO-NPs-AC determined by BET, XRD, FE-SEM, TEM instrument model and other apparatus such as ultrasonic bath, UV–Vis spectrophotometry and pH/Redox/Temperature meter model were used by according to literature [14].

2.2. Experimental apparatus and procedure

Fig. 1 shows the schematic diagram of the setup with ultrasound bath based on following recommendation. 15 mL of MG (5, 10, 15, 20 and 30 mg L⁻¹) in glass flasks in different

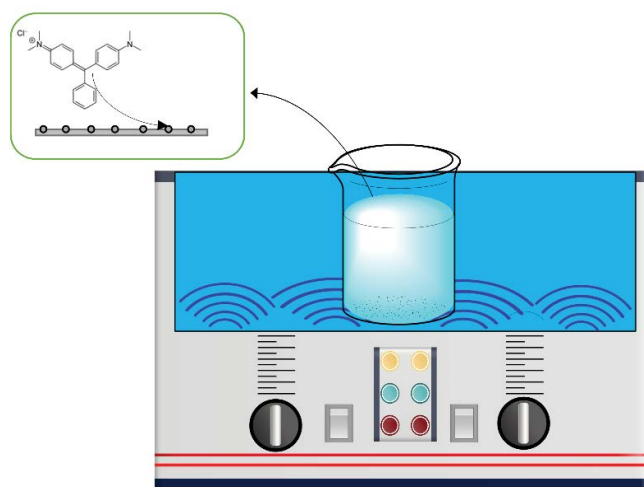
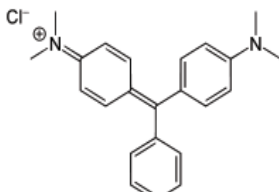


Fig. 1. A schematic diagram of experimental setup with ultrasound bath.

Table 1
Characteristics of the malachite green

Name	Chemical formula	Mw (g mol ⁻¹)	λ_{max} (nm)	Molecular structure
Malachite green	$C_{23}H_{25}ClN_2$ (chloride)	364.911 (chloride)	618	

pH (3–9) was mixed thoroughly with ZnO-NPs-AC and/or AC. The mixture was instantly centrifuged and the spectrum of MG dye in the aqueous solutions was recorded by UV–Vis spectrophotometer, while all experiments were undertaken at room temperature (25°C) in the ultrasonic bath. The MG removal percentage (% MG R) and its adsorbed quantity (q_e (mg g⁻¹)) was calculated according to literature [35–37].

2.3. Response surface design

Response surface methodology (RSM) generally suggest an empirical model which reduce unnecessary experiments and correlated the responses. In the present study, three operational parameters including sonication time (X_1), initial MG concentration (X_2) and adsorbent mass (X_3) was investigated and optimized by CCD (Table 2). The influence of all investigated variables on removal efficiency and prediction of their real behavior and with the detail of the 28 experiments design concern to CCD are represented in Table 3. A polynomial quadratic mathematical model Eq. (2) was used to obtain the optimal conditions and analyzing the effects [38,39].

$$Y\% = \beta_0 + \sum_{i=1}^3 b_i X_i + \sum_{i=1}^3 \sum_{j=1}^3 b_{ij} X_i X_j + \sum_{i=1}^3 b_{ii} X_i^2 + \varepsilon \quad (1)$$

RSM presentation of the interactions among variable for the evaluation of the optimum conditions is obtained with the aid of the experimental data. The significance of independent and dependent variable was judged by p -value and F -value and confirmed by analysis of variance (ANOVA) of the model.

2.4. Artificial neural networks

The ANN is successfully applied for modeling dyes removal from wastewater. In training process, the ANNs are extremely sensitive to the neurons of hidden layer and to improve performance corresponds to three-layer neural model in this study (Fig. 2). The sonication time, MG concentration, and adsorbent dosage known as three neurons in input layer and the output layer is MG removal percentage. In this study, MATLAB (R2013a) software was used to anticipate the MG removal percentage from aqueous solution. The input data were obtained from CCD and all samples were scaled in 0–1 range [40]. The data were accidentally subdivided into two sections (75% and 25% for training and testing set, respectively) and the experimental results (Table 3) were used for ANN modeling technique. The strength of the connections among layers is determined by the amount of weights (w) and biases (b) that the network learns by their

Table 2
Experimental factors and levels in the central composite design

Factor	Levels				
	Low (-1)	Central (0)	High (+1)	- α	+ α
X_1 : Sonication time (min)	3	4	5	2	6
X_2 : Dye concentration (mg L ⁻¹)	10	15	20	5	25
X_3 : Adsorbent dosage (g)	0.01	0.015	0.02	0.005	0.025

Table 3
CCD matrix and responses degradation MG by AC and ZnO-NPs-AC

Run	Block	X_1	X_2	X_3	$P\%_{MG}$	
					Activated carbon	ZnO-NPs-AC
1	1	6	15	0.015	71.03	91
2	1	4	15	0.015	69.21	90.62
3	1	5	10	0.020	69.43	91.54
4	1	4	25	0.015	69.17	77.46
5	1	4	15	0.015	70.82	88.5
6	1	4	15	0.015	69.51	97.65
7	1	5	20	0.010	51.03	92
8	1	2	15	0.015	68.94	82.25
9	1	4	5	0.015	67.98	99.8
10	1	4	15	0.020	62.23	90.87
11	1	3	10	0.010	71.33	91
12	1	4	15	0.015	69.09	94
13	1	4	15	0.005	53.82	63.33
14	1	3	20	0.020	70.53	87
15	1	4	15	0.015	69.12	89.67

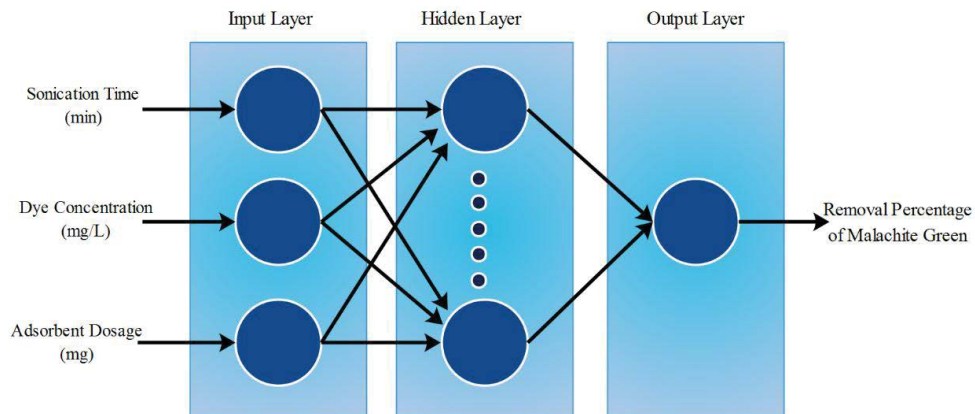


Fig. 2. Structure of a back-propagation artificial network.

adjustment. The tangent sigmoid transfer function (tansig) at hidden layer was used in three-layer feed forward ANN, while linear transfer function (purelin) was used at the output layer. The Levenberg–Marquardt (trainlm) back-propagation (BP) algorithm was applied for training the neural network. The training parameters were 3 input nodes, 5–20 hidden layer neurons, and 1 output node. The best BP algorithm with maximum coefficient of determination (R^2) and minimum mean squared error (MSE) is selected which is effective number of hidden neurons for fitting the model and complexity of network. The optimum ANN architecture model

was specified based on the minimum amount of the MSE of the training and test data set.

3. Result and discussion

3.1. Characterization of ZnO-NPs-AC

FE-SEM images (Figs. 3(a) and (b)) strongly denote surface of the microstructure and morphology and approximate size of ZnO-NPs-AC. The porous characteristics of the ZnO-NPs-AC indicate its well decoration on the AC made from *Ziziphus* wood. FE-SEM of ZnO-NPs-AC (Figs. 3(a) and

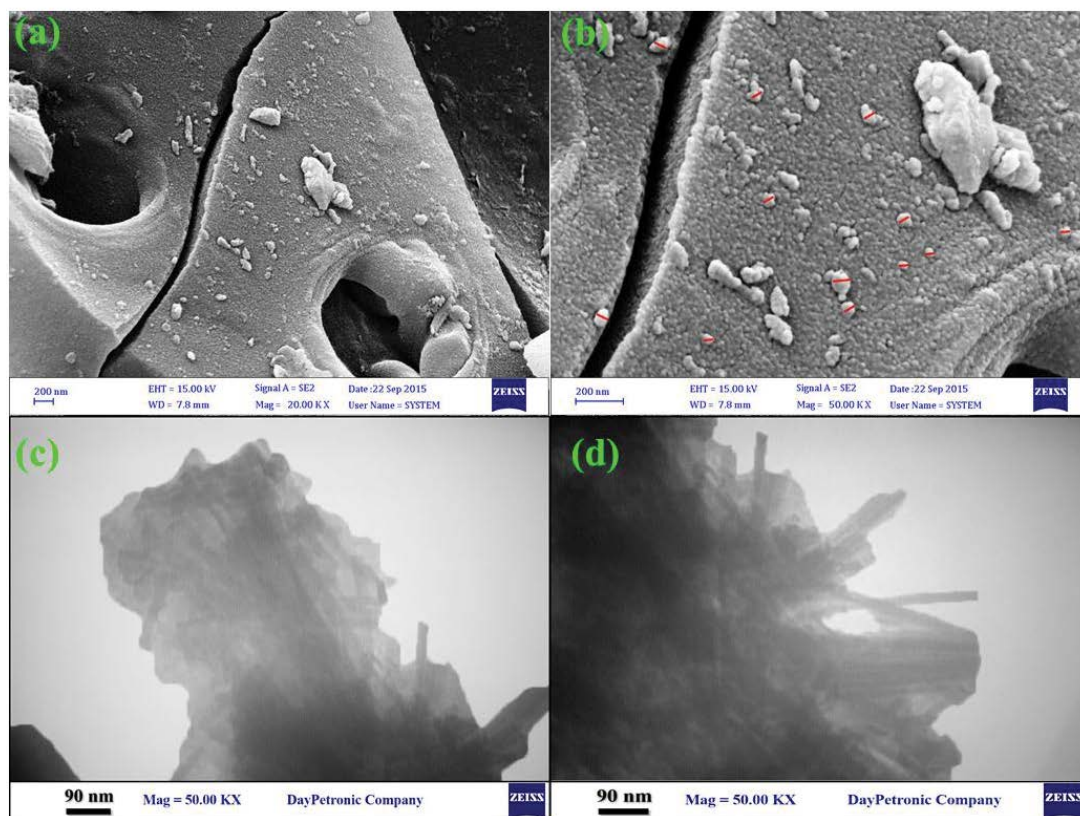


Fig. 3. FE-SEM image of ZnO-NPs-AC (a and b), TEM images of ZnO-NPs-AC (c and d).

(b) show approximate smooth and porous spherical shape with sizes in the range of 50–100 nm. The ZnO-NPs-AC characterized by TEM (Figs. 3(c) and (d)) exhibit hollow space within the inner space and average particle sizes about 20–50 nm.

The XRD pattern of ZnO-NPs-AC (Fig. 4) indicates strong peaks at $2\theta = 31.8^\circ, 34.5^\circ, 36.3^\circ, 47.6^\circ,$ and 56.6° attributed to the (100), (002), (101), (102), and (110) lattice planes of ZnO zincate hexagonal structure and XRD pattern illustrates the presence of ZnO nanoparticles with very small size.

Specific surface area of powder adsorbent as studied by $N_2/77$ K adsorption isotherms gives average pore diameter as 2.763 and 1.165 nm for AC and ZnO-NPs-AC, respectively.

3.2. Effect of pH

The adsorption capacity of ZnO-NPs-AC increased from pH 3.0 to pH 5.0 (Fig. 5) and reached maximum value at pH 5.0 and then the removal percentage held approximately constant thereafter with raising pH. The change in pattern of the ZnO-NPs-AC capacity with pH could be associated

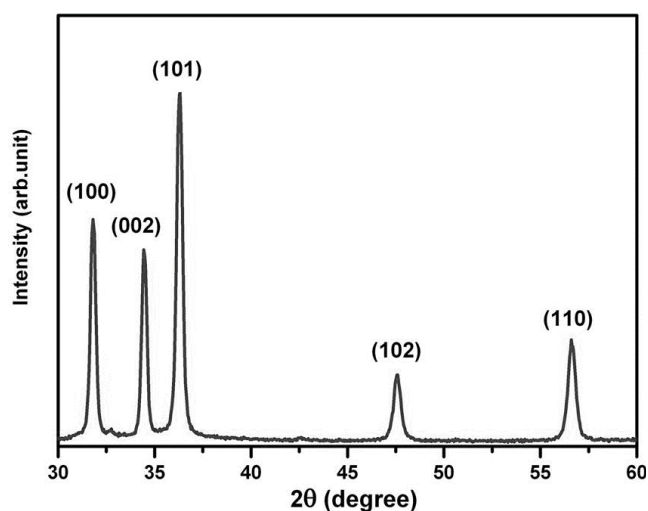


Fig. 4. X-ray diffraction patterns of the prepared ZnO-NPs-AC particles [41].

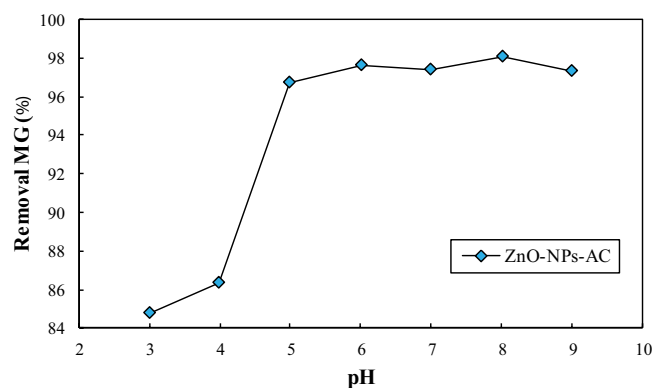


Fig. 5. Effect of pH on removal of binary solution of MG (7 mg L^{-1}) in the pH range of 3–9.

with the effects of pH on the activity of functional groups in the adsorbents and the properties of MG. The MG adsorption onto ZnO-NPs-AC surface is the combination of the various binding mechanism viz. hydrogen bonding, hard interaction and electrostatic forces or through ion–dipole interaction. At acidic solution pH, both adsorbent and MG became positive and significantly high electrostatic repulsion leads to the reduction in MG removal percentages. Gradual increase in pH till 5 leads to disappearance of positive charge and more contribution of hydrogen bonding and ion–dipole and involvement of nonlocalized π electron in accumulation of MG.

3.3. Analysis of CCD

RSM is the impressive method to model and analyze the effect of the main and interactions between variables like $X_1, X_2,$ and X_3 on the adsorption process under few possible conditions by CCD (Table 4). The statistical significance of quadratic model was predicted by the ANOVA based on MG as response and according to results presented in Table 4. The F -value of model for MG removal with AC and ZnO-NPs-AC is 561.99 and 193.41, respectively. The “Lack of fit F -value” of present model for removal of MG dye by AC and ZnO-NPs-AC adsorbent is 5.38 and 2.03, respectively. The analysis of CCD results as determined by design expert software is shown in the following polynomial equation:

$$Y_{R\%MG(AC)} = +69.24 + 0.50X_2 - 1.53X_3 + 0.52X_1 + 5.41X_2X_3 - 5.46X_2X_1 + 5.77X_3X_1 - 4.58X_3^2 + 0.22X_1^2 \quad (2)$$

$$Y_{R\%MG(ZnO-NPs-AC)} = +90.79 - 5.59X_2 + 1.75X_1 + 8.58X_3 + 5.52X_2X_1 + 3.06X_2X_3 - 3.77X_1X_3 - 0.46X_2^2 - 2.50X_3^2 \quad (3)$$

where Y is the adsorption efficiency (%) and $X_1, X_2, X_3, X_2X_3, X_2X_1, X_3X_1, X_3^2,$ and X_1^2 were effects significant for $Y_{R\%MG}$ by AC and for $Y_{R\%MG}$ by ZnO-NPs-AC, the effects of $X_1, X_2, X_3, X_2X_1, X_2X_3, X_1X_3, X_2^2,$ and X_3^2 were significant. The sign of the intercept, linear, quadratic, and interaction coefficients indicates trend of operational parameters influence as positive or negative on the MG removal. Fig. 6(a) shows the predicted results versus actual MG removal adsorption percentage and the measured response results as actual values are in well agreement with the predicted result using the polynomial equations (Eqs. (2) and (3)). The linear relationship between predicted and actual removal percentage by ZnO-NPs-AC and AC in CCD experimental runs with correlation coefficient of $R^2 = 0.9961$ and $R^2 = 0.9987$ (Figs. 6(b) and (c)), respectively.

3.4. Response surface plots

The relationship between statistical operational parameters including effect of independent variables on the dependent variables and their interactions was investigated using three-dimensional (3D) response surface graphs. Figs. 7(a)–(d) indicate the interaction of sonication time, mass of adsorbent and initial MG concentration (AC and ZnO-NPs-AC adsorbent). Amount of adsorbent has positive effect on MG removal percentage and its higher content leads to increase in active surface center sites and more MG accumulation.

Table 4
The results of ANOVA for the response surface quadratic model for MG by AC and ZnO-NPs-AC

Source variation	Activated carbon					ZnO-NPs-AC				
	SS ^a	DF ^b	MS ^c	F-Value	P-Value	SS ^a	DF ^b	MS ^c	F-Value	P-Value
Model	528.64	8	66.08	561.99	<0.0001	1,078.69	8	134.84	193.41	<0.0001
X ₁	2.18	1	2.18	18.57	0.0050	24.50	1	24.50	35.14	0.0010
X ₂	2.04	1	2.04	17.35	0.0059	249.54	1	249.54	357.93	<0.0001
X ₃	5.36	1	5.36	45.62	0.0005	589.27	1	589.27	845.25	<0.0001
X ₁ X ₂	43.51	1	43.51	370.06	<0.0001	81.25	1	81.25	116.55	<0.0001
X ₁ X ₃	88.86	1	88.86	755.72	<0.0001	25.01	1	25.01	35.87	0.0010
X ₂ X ₃	77.90	1	77.90	662.56	<0.0001	37.95	1	37.95	54.44	0.0003
X ₁ ²	1.19	1	1.19	10.09	0.0192	–	–	–	–	–
X ₂ ²	–	–	–	–	–	5.45	1	5.45	7.81	0.0314
X ₃ ²	149.36	1	149.36	1,270.25	<0.0001	157.72	1	157.72	226.22	<0.0001
Residual	0.71	6	0.12			4.18	6	0.70		
Lack of fit	0.51	2	0.26	5.38	0.0734	2.11	2	1.05	2.03	0.2458
Pure error	0.19	4	0.048			2.07	4	0.52		
Cor. total	529.34	14				1,082.87	14			

	Std. Dev.	Mean	C.V. %	PRESS	R ²	Adj. R ²	Pred. R ²	Adeq. Precision
AC	0.34	66.77	0.51	39.96	0.998	0.996	0.924	76.628
ZnO-NPs-AC	0.83	88.42	0.94	234.61	0.996	0.991	0.783	56.404

^aSum of square; ^bDegree of freedom; ^cMean of square.

At lower mass, due to a reduction in the number of active sites and nonsufficient available surface area leads to strong reduction in removal percentage (Fig. 7(a)). Also can be seen (Fig. 7(d)) elevating the value of adsorbent from 0.004 to 0.026 g is proportional with improvement of MG removal percentages. Typically sonication time effect on the removal of MG by AC and ZnO-NPs-AC (Figs. 7(b) and (d)) is owing to more mixing of adsorbent with solution and more subsequent mass transfer, which leads to more and efficient accumulation of MG in short sonication time that extremely support high contribution of ultrasound power. High concentration of MG is proportional and relevant to lower available and empty active surface site than MG dye molecule and cause more decrease in MG removal percentage.

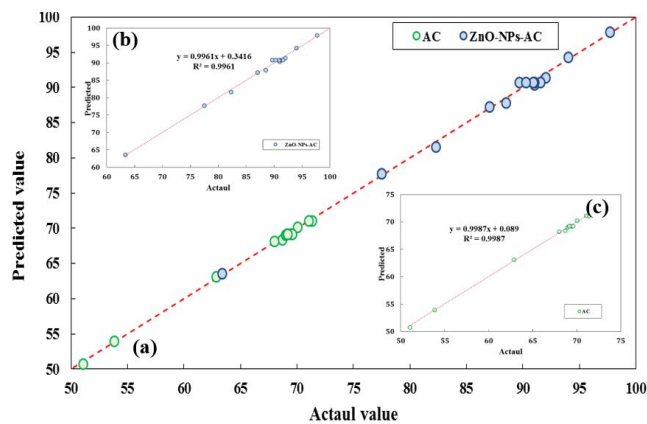


Fig. 6. Predicted value versus actual value for adsorption of MG dye by (a) AC and ZnO-NPs-AC, (b) ZnO-NPs-AC, (c) AC.

3.5. Optimization of CCD for MG

The profile desirable responses for MG removal percentage by AC and ZnO-NPs-AC (Fig. 8) reveal that current level of each variable (X₁, X₂, and X₃) in the model was illustrated at the bottom of Fig. 8 while MG removal percentage is shown in left-hand side of Fig. 8. The optimum conditions were found to be pH 8.0, 4.65 min sonication, which lead to

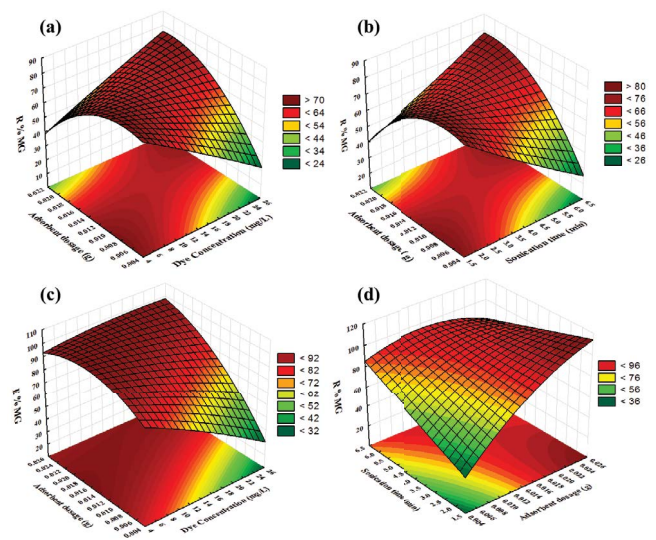


Fig. 7. Response plots for X₂X₃ for the removal of MG dye (a), X₁X₃ for the removal of MG dye (b) by activated carbon, X₂X₃ for the removal of MG dye (c), X₁X₃ for the removal of MG dye (d) by ZnO-NPs-AC.

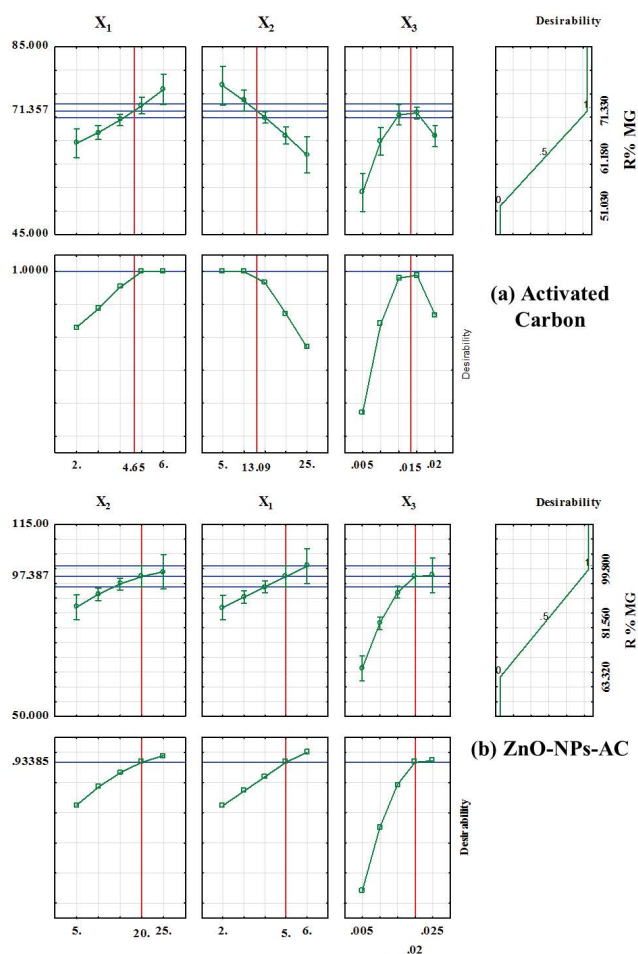


Fig. 8. Profile for predicted values and desirability function for simultaneous removal percentage of MG dye by activated carbon (a), ZnO-NPs-AC (b).

accumulation of 71.35% MG onto 0.015 g AC. On the other hand, after 5 min sonication for mixing sample of 20 mg L⁻¹ of MG lead to quantitative accumulation of MG onto 0.02 g ZnO-NPs-AC with removal percentage more than 97%.

3.6. ANN modeling

ANN model was applied for modeling of MG adsorption systems and to correlate effect of the three input variables including sonication time (X_1), MG concentration (X_2), and adsorbent mass (X_3) on MG removal percentage as output. The experimental data obtained under various conditions were used to train and test the neural network. The ANN structure has three inputs and output layer and the optimal ANN architecture optimize one hidden layer with eight neurons (3-8-1) and training algorithm for AC and ZnO-NP-AC is Levenberg–Marquardt. The well-operation parameters was considered by selecting the optimal one based on coefficient of determination (R^2) maximization and MSE minimization with training various ANN architecture. As seen in Table 5, the best ANN network performance could predict the R^2 of 0.9999 and 0.9999 for training and testing sample of MG onto AC and 0.9994 and 0.9970 for training and testing sample of MG onto ZnO-NPs-AC. The MSE of 2.85E-04 and 0.00116 for training and testing of MG over AC adsorbent, respectively, 3.47E-03 and 0.01789 for training and testing of MG over ZnO-NPs-AC adsorbent, respectively. The result confirms the compatibility evaluation based on ANN model for forecasting experimental adsorption data. Figs. 9(a) and (b) show that the scatter plot of the ANN model predicted versus experimental data of MG dye removal by AC and ZnO-NPs-AC adsorbent that the goodness of fit between all forecast values for the removal MG of data using the ANN model and experimental data. The MSE versus epochs of the best neural network for each sample is inset in Figs. 9(a) and (b) and five iterations for MG onto AC and ZnO-NPs-AC, model has the lowest value of MSE in training network.

Table 5
Dependence between neuron numbers at hidden layer with MSE and R^2

Number of neurons	AC				ZnO-NPs-AC			
	Train		Test		Train		Test	
	MSE	R^2	MSE	R^2	MSE	R^2	MSE	R^2
5	3.24E-04	0.9999	0.07578	0.9928	3.13E-03	0.9994	0.20111	0.9633
6	4.18E-04	0.9999	0.4492	0.9577	3.29E-03	0.9994	0.84566	0.8339
7	4.69E-04	0.9999	0.3417	0.9622	3.79E-03	0.9993	0.13522	0.9746
8	2.85E-04	0.9999	0.00116	0.9999	3.47E-03	0.9994	0.01789	0.9970
9	2.43E-05	0.9999	0.3305	0.9693	2.69E03	0.9995	0.80752	0.8492
10	4.18E-04	0.9999	0.11673	0.9889	3.29E-03	0.9994	0.21697	0.9618
11	2.42E-05	0.9999	0.08747	0.9926	2.18E-03	0.9996	0.14265	0.9787
12	2.43E-05	0.9999	0.70715	0.9250	2.69E-03	0.9995	0.36286	0.9324
13	4.11E-04	0.9999	0.05831	0.9945	3.47E-03	0.9994	0.08482	0.9847
14	3.23E-04	0.9999	0.00704	0.9993	3.13E-03	0.9994	0.02837	0.9945
15	4.69E-04	0.9969	0.09627	0.9908	3.79E-03	0.9993	0.31174	0.9428
20	183E-05	0.9999	0.05185	0.9954	2.59E-03	0.9995	0.10593	0.9826

Bold is an indicator of best model.

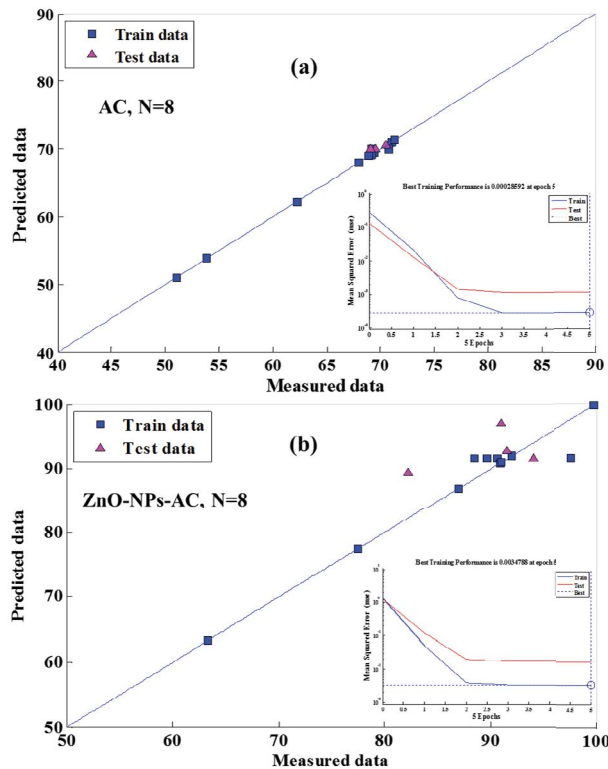


Fig. 9. A scatter plot of the ANN predicted versus experimental data of MG dye removal by AC (a) and ZnO-NPs-AC (b) (the MSE vs epochs of the best neural network for each sample is inset in this figure).

3.7. Adsorption equilibrium study

The equilibrium adsorption isotherms have substantial knowledge in determining the adsorbent–adsorbate interaction kinetics and mechanism of adsorption of MG. Equilibrium isotherm models were studied and

their parameters for the adsorption of MG onto AC and ZnO-NPs-AC correspond to conventional Langmuir [42], Freundlich [43], Temkin [44], and Dubinin–Radushkevich (D-R) [45] isotherm models in addition to their correlation coefficients (R^2) presented in Table 6. The Langmuir adsorption based on monolayer MG onto AC and ZnO-NPs-AC is judged according to the values of K_a (the Langmuir adsorption constant (L mg^{-1}) and q_m (the theoretical maximum adsorption capacity of adsorbent (mg g^{-1})) which as mentioned previously can be calculated from the intercept and slope of the linear plot of C_e/q_e versus C_e , respectively [46]. The high correlation ($R^2 = 0.9941$ and 0.9991) coefficient indicates that Langmuir adsorption isotherms are suitable for the interpretation of MG adsorption onto AC and ZnO-NPs-AC over the whole applied concentration range. An adsorption isotherm for a heterogeneous adsorbent surface is described on the basis of Freundlich adsorption isotherm model [47,48]. In present model $1/n$ (the capacity and intensity of the dye adsorption onto the adsorbent) and K_F (Freundlich coefficients ($(\text{mg g}^{-1})/(\text{mg L}^{-1})^{1/n}$)) were calculated from the slope and intercept of the linear plot of $\ln q_e$ versus $\ln C_e$, respectively. Thus, the low correlation coefficient illustrates the poor agreement of the experimental data with Freundlich isotherm model. The value of $1/n$ in AC and ZnO-NPs-AC are below 1 that indicates favorable adsorption condition. The heat of the adsorption by using Temkin isotherm model was calculated [49]. B is the Temkin constant related to heat of the adsorption (J mol^{-1}), and K_T is the equilibrium binding constant (L mg^{-1}), T is the absolute temperature (K), and R is the universal gas constant ($8.314 \text{ J mol}^{-1} \text{ K}^{-1}$) [50]. The D-R isotherm model was also applied to evaluate the free energy and the specifications of adsorbents [51,52]. K is a constant related to the adsorption energy ($\text{mol}^2 (\text{kJ}^2)^{-1}$), q_m is the theoretical saturation capacity (mg g^{-1}), ϵ is the Polanyi potential. The values of K and q_m were calculated from the slope and intercept of the linear plot of $\ln q_e$ versus ϵ^2 , respectively [53]. The values of the correlation coefficient (R^2) for D-R model (0.929 and 0.943 for adsorption removal of MG onto AC and ZnO-NPs-AC, respectively) are lower than the Freundlich,

Table 6

Various isotherm constants and their correlation coefficients calculated for the adsorption of MG onto AC and ZnO-NPs-AC

Isotherm	Equation	Parameters	Activated carbon	ZnO-NPs-AC
Langmuir	$q_e = q_m K_a C_e / (1 + K_a C_e)$	q_m (mg g^{-1})	65.04	92.6
		K_a (L mg^{-1})	0.143	1.30
		R^2	0.994	0.999
Freundlich	$\ln q_e = \ln K_F + (1/n) \ln C_e$	$1/n$	0.635	0.455
		K_F (L mg^{-1})	2.588	5.13
		R^2	0.979	0.967
Temkin	$q_e = B_1 \ln K_T + B_1 \ln C_e$	B_1	14.081	18.824
		K_T (L mg^{-1})	1.49	14.974
		R^2	0.992	0.991
Dubinin–Radushkevich (D-R)	$\ln q_e = \ln Q_s - B\epsilon^2$	Q_s (mg g^{-1})	36.73	53
		B	−6E-7	−6E-8
		ϵ (kJ mol^{-1})	912.24	2,890.1
		R^2	0.929	0.943

Langmuir, and Temkin values. Therefore, the D-R isotherm demonstrates a worse fit of experimental equilibrium data than other isotherms adsorption for removal of MG dye in system.

3.8. Adsorption kinetics study

The analysis of adsorption kinetics correspond to MG accumulation onto AC and ZnO-NP-AC was investigated using three kinetic models including the pseudo-first-order, pseudo-second-order, [54], and intraparticle diffusion [55] models at various adsorbent dosage at optimum value of sonication time and pH. Table 7 shows the constant parameters of each model for removal of MG dye by AC and ZnO-NP-AC in aqueous solution for linear pseudo-first-order equation (Lagergren model) as follows [56,57]:

$$\log(q_e - q_t) = \log q_e - k_1 t / 2.303 \quad (4)$$

The values of k_1 and q_e were calculated from the slope and intercept of the linear plot of $\log(q_e - q_t)$ versus t , respectively and R^2 is correlation coefficients (Table 7). It was observed that the pseudo-first-order did not fit well and the calculated q_e values do not agree with the experimental q_e value. Because of the adsorption of MG onto AC and ZnO-NPs-AC, it does not follow pseudo-first-order kinetic equation. The pseudo-second-order kinetic equation is as follows [58]:

$$\frac{t}{q_t} = \frac{1}{k_2 q_e^2} + \frac{t}{q_e} \quad (5)$$

where q_e and q_t are the MG adsorption capacity on AC and ZnO-NP-AC at equilibrium and at t (min), respectively, and k_2 is the rate constant for the second-order kinetic model. The values of k_2 and q_e were calculated from the intercept and slope of line plotting correspond to t/q_t versus t , respectively. The intraparticle diffusion equation is generally expressed as follows [59]:

$$q_t = K_{\text{diff}} t^{1/2} + C \quad (6)$$

where q_t is the sorption capacity on AC and ZnO-NP-AC at time t (min), K_{diff} is the intraparticle diffusion rate constant ($\text{mg g}^{-1} \text{min}^{-1/2}$), and C is the thickness of the boundary layer. In Weber and Morris theory the plot between q_t versus $t^{1/2}$ is

given by several areas representing the various steps participated in the adsorption process [60]. If the regression of q_t versus $t^{1/2}$ is linear or correlation coefficient value is near to 1 is proportional with the fact that intraparticle diffusion is the rate-limiting step. The values of R^2 for the pseudo-first-order (0.9082 and 0.9279), the pseudo-second-order (0.9857 and 0.9943), and intraparticle diffusion (0.9142 and 0.9435) kinetic models (Table 7) for MG adsorption onto AC and ZnO-NPs-AC, respectively. On the other hand, the values of R^2 for the pseudo-second-order kinetic model were most suitable and closeness of experimental data.

4. Conclusion

The present investigation indicated that *Ziziphus* wood can be effectively used as a raw matter for the preparation of AC and ZnO nanoparticles loaded on AC as an adsorbent for the removal of MG from aqueous media performed with four various variables (pH, adsorbent dosage, sonication time, and MG concentration). The ANN and RSM models were made for predicting the MG removal percentage and adsorbent was characterized using FE-SEM, TEM, XRD, and BET analysis. The experimental data were fitted to the RSM model and relationship among the response and the variables was expressed by a polynomial equation. The optimization of process was performed using CCD under RSM and the results indicate desirable efficiency of about 71.35% using AC under pH of 8.0, 0.015 g of adsorbent, 13.09 mg L^{-1} of MG at 4.65 min sonication and best operational condition for ZnO-NPs-AC was pH of 8.0, 0.02 g of adsorbent, 20 mg L^{-1} of MG at 5 min sonication which lead to improvement in removal percentage to 97.38%. The ANN model was used to simulate and model adsorption of MG using AC and ZnO-NPs-AC. A three-layer ANN model with tansig transfer function at hidden layer with eight neurons is more suitable to predict the MG adsorption onto AC and ZnO-NPs-AC, respectively. The isotherm equilibrium data were best described by the Temkin isotherm model for AC adsorbent and Langmuir for ZnO-NPs-AC adsorbent. The adsorption kinetics excellently was fitted to pseudo-second-order kinetic model for both adsorbents and experimental results confirm adsorbent ability to remove large quantity of MG dye (20 mg L^{-1}) in short time (5 min) using little amount of lower toxicity of ZnO and natural source AC (*Ziziphus* wood).

Table 7
Kinetic parameters for the adsorption of dye onto ZnO-NPs-AC and AC in 0.15 mg L^{-1} of dye

Model	Parameters	Activated carbon	ZnO-NPs-AC
Pseudo-first-order kinetic	k_1 (min^{-1})	0.47	0.501
	q_e (calc) (mg g^{-1})	21.1	25.67
	R^2	0.9082	0.9279
Pseudo-second-order kinetic	k_2 (min^{-1})	0.025	0.024
	q_e (calc) (mg g^{-1})	38.02	52.35
	R^2	0.9857	0.9943
Intraparticle diffusion	K_{diff} ($\text{mg g}^{-1} \text{min}^{-1/2}$)	6.22	7.46
	C (g mg^{-1})	17.28	28.45
	R^2	0.9142	0.9435
	q_e (mg g^{-1})	33.23	47.27

References

- [1] A.S. ALZaydien, Adsorption of methylene blue from aqueous solution onto a low-cost natural Jordanian Tripoli, *Am. J. Appl. Sci.*, 6 (2009) 1047.
- [2] Y.-S. Ho, T.-H. Chiang, Y.-M. Hsueh, Removal of basic dye from aqueous solution using tree fern as a biosorbent, *Process Biochem.*, 40 (2005) 119–124.
- [3] M. Roosta, M. Ghaedi, A. Daneshfar, R. Sahraei, A. Asghari, Optimization of the ultrasonic assisted removal of methylene blue by gold nanoparticles loaded on activated carbon using experimental design methodology, *Ultrason. Sonochem.*, 21 (2014) 242–252.
- [4] S.J. Culp, F.A. Beland, Malachite green: a toxicological review, *Int. J. Toxicol.*, 15 (1996) 219–238.
- [5] S. Srivastava, R. Sinha, D. Roy, Toxicological effects of malachite green, *Aquat. Toxicol.*, 66 (2004) 319–329.
- [6] S. Chowdhury, P. Saha, Sea shell powder as a new adsorbent to remove Basic Green 4 (Malachite Green) from aqueous solutions: equilibrium, kinetic and thermodynamic studies, *Chem. Eng. J.*, 164 (2010) 168–177.
- [7] B.K. Sinha, Free radicals in anticancer drug pharmacology, *Chem. Biol. Interact.*, 69 (1989) 293–317.
- [8] R. Han, J. Zhang, W. Zou, J. Shi, H. Liu, Equilibrium biosorption isotherm for lead ion on chaff, *J. Hazard. Mater.*, 125 (2005) 266–271.
- [9] A. Sari, D. Mendil, M. Tuzen, M. Soylak, Biosorption of Cd (II) and Cr (III) from aqueous solution by moss (*Hylocomium splendens*) biomass: equilibrium, kinetic and thermodynamic studies, *Chem. Eng. J.*, 144 (2008) 1–9.
- [10] R. Dolphen, N. Sakkayawong, P. Thiravetyan, W. Nakbanpote, Adsorption of Reactive Red 141 from wastewater onto modified chitin, *J. Hazard. Mater.*, 145 (2007) 250–255.
- [11] S. Sachdeva, A. Kumar, Preparation of nanoporous composite carbon membrane for separation of rhodamine B dye, *J. Membr. Sci.*, 329 (2009) 2–10.
- [12] V.K. Gupta, R. Jain, S. Varshney, Electrochemical removal of the hazardous dye Reactifox Red 3 BFN from industrial effluents, *J. Colloid Interface Sci.*, 312 (2007) 292–296.
- [13] J.M. Dias, M.C.M. Alvim-Ferraz, M.F. Almeida, J. Rivera-Utrilla, M. Sánchez-Polo, Waste materials for activated carbon preparation and its use in aqueous-phase treatment: a review, *J. Environ. Manage.*, 85 (2007) 833–846.
- [14] A. Daneshyar, M. Ghaedi, M.M. Sabzehmeidani, A. Daneshyar, {H₂S} adsorption onto Cu-Zn-Ni nanoparticles loaded activated carbon and Ni-Co nanoparticles loaded γ -Al₂O₃: optimization and adsorption isotherms, *J. Colloid Interface Sci.*, 490 (2017) 553–561.
- [15] J. Avom, J.K. Mbadcam, C. Noubactep, P. Germain, Adsorption of methylene blue from an aqueous solution on to activated carbons from palm-tree cobs, *Carbon N.Y.*, 35 (1997) 365–369.
- [16] N. Yalçın, V. Sevinc, Studies of the surface area and porosity of activated carbons prepared from rice husks, *Carbon N.Y.*, 38 (2000) 1943–1945.
- [17] A.H. El-Sheikh, A.P. Newman, H.K. Al-Daffaee, S. Phull, N. Cresswell, Characterization of activated carbon prepared from a single cultivar of Jordanian Olive stones by chemical and physicochemical techniques, *J. Anal. Appl. Pyrolysis.*, 71 (2004) 151–164.
- [18] W.T. Tsai, C.Y. Chang, M.C. Lin, S.F. Chien, H.F. Sun, M.F. Hsieh, Adsorption of acid dye onto activated carbons prepared from agricultural waste bagasse by ZnCl₂ activation, *Chemosphere*, 45 (2001) 51–58.
- [19] S. Sivakumar, P. Senthilkumar, V. Subburam, Carbon from cassava peel, an agricultural waste, as an adsorbent in the removal of dyes and metal ions from aqueous solution, *Bioresour. Technol.*, 80 (2001) 233–235.
- [20] S. Senthilkumaar, P.R. Varadarajan, K. Porkodi, C.V. Subbhuraam, Adsorption of methylene blue onto jute fiber carbon: kinetics and equilibrium studies, *J. Colloid Interface Sci.*, 284 (2005) 78–82.
- [21] B.S. Girgis, A.-N.A. El-Hendawy, Porosity development in activated carbons obtained from date pits under chemical activation with phosphoric acid, *Microporous Mesoporous Mater.*, 52 (2002) 105–117.
- [22] H. Jamshidi, M. Ghaedi, M.M. Sabzehmeidani, A.R. Bagheri, Comparative study of acid yellow 119 adsorption onto activated carbon prepared from lemon wood and ZnO nanoparticles loaded on activated carbon, *Appl. Organomet. Chem.*, (n.d.) e4080, doi:10.1002/aoc.4080.
- [23] E. Unur, Functional nanoporous carbons from hydrothermally treated biomass for environmental purification, *Microporous Mesoporous Mater.*, 168 (2013) 92–101.
- [24] M. Ghaedi, H. Tavallali, M. Sharifi, S.N. Kokhdan, A. Asghari, Preparation of low cost activated carbon from *Myrtus communis* and pomegranate and their efficient application for removal of Congo red from aqueous solution, *Spectrochim. Acta, Part A*, 86 (2012) 107–114.
- [25] M. Ghaedi, M. Pakniat, Z. Mahmoudi, S. Hajati, R. Sahraei, A. Daneshfar, Synthesis of nickel sulfide nanoparticles loaded on activated carbon as a novel adsorbent for the competitive removal of Methylene blue and Safranin-O, *Spectrochim. Acta, Part A*, 123 (2014) 402–409.
- [26] N.G. Waller, H.A. Kaiser, J.B. Illian, M. Manry, A comparison of the classification capabilities of the 1-dimensional Kohonen neural network with two partitioning and three hierarchical cluster analysis algorithms, *Psychometrika*, 63 (1998) 5–22.
- [27] Ö. Kişi, River flow modeling using artificial neural networks, *J. Hydrol. Eng.*, 9 (2004) 60–63.
- [28] S. Elemen, E.P.A. Kumbasar, S. Yapar, Modeling the adsorption of textile dye on organoclay using an artificial neural network, *Dyes Pigm.*, 95 (2012) 102–111.
- [29] M. Maghsoudi, M. Ghaedi, A. Zinali, A.M. Ghaedi, M.H. Habibi, Artificial neural network (ANN) method for modeling of sunset yellow dye adsorption using zinc oxide nanorods loaded on activated carbon: kinetic and isotherm study, *Spectrochim. Acta, Part A*, 134 (2015) 1–9.
- [30] A.M. Ghaedi, A. Vafaei, Applications of artificial neural networks for adsorption removal of dyes from aqueous solution: a review, *Adv. Colloid Interface Sci.*, 245 (2017) 20–39.
- [31] U. Yurtsever, M. Yurtsever, İ.A. Şengil, N. Kıratlı Yılmazçoban, Fast artificial neural network (FANN) modeling of Cd (II) ions removal by valonia resin, *Desal. Wat. Treat.*, 56 (2015) 83–96.
- [32] F. Ruggieri, A.A. D'Archivio, G. Carlucci, P. Mazzeo, Application of artificial neural networks for prediction of retention factors of triazine herbicides in reversed-phase liquid chromatography, *J. Chromatogr., A*, 1076 (2005) 163–169.
- [33] D. Salari, N. Daneshvar, F. Aghazadeh, A.R. Khataee, Application of artificial neural networks for modeling of the treatment of wastewater contaminated with methyl tert-butyl ether (MTBE) by UV/H₂O₂ process, *J. Hazard. Mater.*, 125 (2005) 205–210.
- [34] Y. Kikuchi, Q. Qian, M. Machida, H. Tatsumoto, Effect of ZnO loading to activated carbon on Pb (II) adsorption from aqueous solution, *Carbon N.Y.*, 44 (2006) 195–202.
- [35] A. Asfaram, M. Ghaedi, S. Agarwal, I. Tyagi, V.K. Gupta, Removal of basic dye Auramine-O by ZnS: Cu nanoparticles loaded on activated carbon: optimization of parameters using response surface methodology with central composite design, *RSC Adv.*, 5 (2015) 18438–18450.
- [36] R. Mimouni, K. Boubaker, M. Amlouk, Investigation of structural and optical properties in Cobalt-Chromium co-doped ZnO thin films within the Lattice Compatibility Theory scope, *J. Alloys Compd.*, 624 (2015) 189–194.
- [37] K. Dashtian, S. Porhemat, A.R. Rezvani, M. Ghaedi, M.M. Sabzehmeidani, Adsorption of semisoft pollutants onto Bi₂S₃/Ag₂S-AC under the influence of ultrasonic waves as external field, *J. Ind. Eng. Chem.*, 60 (2018) 390–400.
- [38] K. Dashtian, M. Ghaedi, M.M. Sabzehmeidani, E. Ameri, Novel visible light-driven Cu-based MOFs/Ag₂O composite photocatalysts with enhanced photocatalytic activity toward the degradation of orange G: its photocatalytic mechanism and optimization study, *New J. Chem.*, 42 (2018) 9720–9734.

- [39] M.M. Sabzehmeidani, H. Karimi, M. Ghaedi, Electrospinning preparation of NiO/ZnO composite nanofibers for photo-degradation of binary mixture of rhodamine B and methylene blue in aqueous solution: central composite optimization, *Appl. Organomet. Chem.*, 32 (2018) e4335.
- [40] A.R. Khataee, M.B. Kasiri, Artificial neural networks modeling of contaminated water treatment processes by homogeneous and heterogeneous nanocatalysis, *J. Mol. Catal. A: Chem.*, 331 (2010) 86–100.
- [41] M. Ghaedi, F.N. Azad, K. Dashtian, S. Hajati, A. Goudarzi, M. Soylak, Central composite design and genetic algorithm applied for the optimization of ultrasonic-assisted removal of malachite green by ZnO Nanorod-loaded activated carbon, *Spectrochim. Acta, Part A*, 167 (2016) 157–164.
- [42] A. Shamsizadeh, M. Ghaedi, A. Ansari, S. Azizian, M.K. Purkait, Tin oxide nanoparticle loaded on activated carbon as new adsorbent for efficient removal of malachite green-oxalate: non-linear kinetics and isotherm study, *J. Mol. Liq.*, 195 (2014) 212–218.
- [43] K. Porkodi, K.V. Kumar, Equilibrium, kinetics and mechanism modeling and simulation of basic and acid dyes sorption onto jute fiber carbon: Eosin yellow, malachite green and crystal violet single component systems, *J. Hazard. Mater.*, 143 (2007) 311–327.
- [44] İ. Küncekk, S. Şener, Adsorption of methylene blue onto sonicated sepiolite from aqueous solutions, *Ultrason. Sonochem.*, 17 (2010) 250–257.
- [45] S.R. Shirsath, A.P. Patil, R. Patil, J.B. Naik, P.R. Gogate, S.H. Sonawane, Removal of Brilliant Green from wastewater using conventional and ultrasonically prepared poly (acrylic acid) hydrogel loaded with kaolin clay: a comparative study, *Ultrason. Sonochem.*, 20 (2013) 914–923.
- [46] H.I. Chieng, N. Priyantha, L.B.L. Lim, Effective adsorption of toxic brilliant green from aqueous solution using peat of Brunei Darussalam: isotherms, thermodynamics, kinetics and regeneration studies, *RSC Adv.*, 5 (2015) 34603–34615.
- [47] L. Sun, S. Wan, W. Luo, Biochars prepared from anaerobic digestion residue, palm bark, and eucalyptus for adsorption of cationic methylene blue dye: characterization, equilibrium, and kinetic studies, *Bioresour. Technol.*, 140 (2013) 406–413.
- [48] R.K. Ghosh, D.D. Reddy, Crop residue ashes as adsorbents for basic dye (methylene blue) removal: adsorption kinetics and dynamics, *Clean – Soil, Air, Water*, 42 (2014) 1098–1105.
- [49] J.H. De Boer, Adsorption phenomena, *Adv. Catal.*, 8 (1956) 17–161.
- [50] I.B. Alstrup, J.R. Rostrup-Nielsen, S. Røen, High temperature hydrogen sulfide chemisorption on nickel catalysts, *Appl. Catal.*, 1 (1981) 303–314.
- [51] M.M. Dubinin, The potential theory of adsorption of gases and vapors on carbon adsorbents with energetically nonuniform surfaces., *Chem. Rev.*, 60 (1960) 235–241.
- [52] M.M. Dubinin, Modern state of the theory of volume filling of micropore adsorbents during adsorption of gases and steams on carbon adsorbents, *Zh. Fiz. Khim.*, 39 (1965) 1305–1317.
- [53] A. Özcan, E.M. Öncü, A.S. Özcan, Kinetics, isotherm and thermodynamic studies of adsorption of Acid Blue 193 from aqueous solutions onto natural sepiolite, *Colloids Surf., A*, 277 (2006) 90–97.
- [54] T. Yan, L. Wang, Adsorption of CI Reactive Red 228 and Congo Red dye from aqueous solution by amino-functionalized Fe₃O₄ particles: kinetics, equilibrium, and thermodynamics, *Water Sci. Technol.*, 69 (2014) 612–621.
- [55] Z. Ioannou, J. Simitzis, Adsorption of methylene blue dye onto activated carbons based on agricultural by-products: equilibrium and kinetic studies, *Water Sci. Technol.*, 67 (2013) 1688–1694.
- [56] S. Dridi-Dhaouadi, N. Ben Douissa-Lazreg, M.F. M’Henni, Removal of lead and Yellow 44 acid dye in single and binary component systems by raw *Posidonia oceanica* and the cellulose extracted from the raw biomass, *Environ. Technol.*, 32 (2011) 325–340.
- [57] S. Nethaji, A. Sivasamy, Adsorptive removal of an acid dye by lignocellulosic waste biomass activated carbon: equilibrium and kinetic studies, *Chemosphere*, 82 (2011) 1367–1372.
- [58] A. Pourjavadi, M. Nazari, B. Kabiri, S.H. Hosseini, C. Bennett, Preparation of porous graphene oxide/hydrogel nanocomposites and their ability for efficient adsorption of methylene blue, *RSC Adv.*, 6 (2016) 10430–10437.
- [59] S. Çoruh, F. Geyikçi, O. Nuri Ergun, Adsorption of basic dye from wastewater using raw and activated red mud, *Environ. Technol.*, 32 (2011) 1183–1193.
- [60] W. Konicki, I. Pelech, E. Mijowska, I. Jasińska, Adsorption kinetics of acid dye acid Red 88 onto magnetic multi-walled carbon nanotubes-Fe₃C nanocomposite, *Clean – Soil, Air, Water*, 42 (2014) 284–294.